Temporal X-ray Reconstruction using Temporal and Spectral Measurements at LCLS

Florian Christie,[1,2,*] Alberto Andrea Lutman,[3] Yuantao Ding,[3] Zhirong Huang,[3] Vatsal A. Jhalani,[3,†] Jacek Krzywinski,[3] Timothy John Maxwell,[3] Daniel Ratner,[3] Juliane Rönsch-Schulenburg,[1] and Mathias Vogt[1]

[1] *Deutsches Elektronen-Synchrotron, 22607 Hamburg, Germany*
[2] *Universität Hamburg, 22607 Hamburg, Germany.*
[3] *SLAC National Accelerator Laboratory, Menlo Park, California 94025, USA*

(Dated: January 20, 2022)

Transverse deflecting structures (TDS) are widely used in accelerator physics to measure the longitudinal density of particle bunches. When used in combination with a dispersive section, the whole longitudinal phase space density can be imaged. At the Linac Coherent Light Source (LCLS), the installation of such a device downstream of the undulators enables the reconstruction of the X-ray temporal intensity profile by comparing longitudinal phase space distributions with lasing on and lasing off. However, the resolution of this TDS is limited to around 1 fs rms (root mean square), and therefore, it is not possible to resolve single self-amplified spontaneous emission (SASE) spikes within one X-ray photon pulse. By combining the power spectrum from a high resolution photon spectrometer and the temporal structure from the TDS, the overall resolution is enhanced, thus allowing the observation of temporal, single SASE spikes. The combined data from the spectrometer and the TDS is analyzed using an iterative algorithm to obtain the actual intensity profile. In this paper, we present some improvements to the reconstruction algorithm as well as real data taken at LCLS.

arXiv:1911.06090v2 [physics.acc-ph] 7 Jul 2020

I. INTRODUCTION

Transverse deflecting structures (TDS) are used to time-resolve the electron bunch phase spaces downstream of an X-ray free-electron laser (FEL) undulator line to measure the electron bunch energy losses induced by the lasing process [1]. The electron bunch time-resolved losses match the emitted X-ray temporal profile [2], and therefore TDSs are routinely used as diagnostics to measure the X-ray pulse profiles [1]. However, the limited resolution of a measurement using a TDS imposes an upper limit on the resolution of the temporal reconstruction of photon pulses. As the resolution of an X-band TDS used at an X-ray FEL is typically limited to around 1 fs rms (root mean square), single self-amplified spontaneous emission (SASE) spikes, typically in the range of 0.1 fs to 3 fs, within one photon pulse can often not be resolved. However, the exact knowledge of the temporal structure of SASE radiation is interesting for applications such as "ghost imaging" [3].

By combining the power spectrum from a high resolution photon spectrometer [4] and the temporal structure from the TDS, the overall resolution can be enhanced, thus allowing the observation of temporal, single SASE spikes in the X-ray range. The combined data from the spectrometer and the TDS is analyzed using an iterative algorithm to obtain an estimate of the actual intensity profile. This iterative reconstruction algorithm is published in [5, 6].

In the following, we will discuss some improvements and adjustments to this iterative reconstruction algorithm that are necessary to analyze real data due to the spectrometer resolution of 0.2 eV during the measurements.

II. ADJUSTMENTS TO ITERATIVE RECONSTRUCTION ALGORITHM

The iterative reconstruction algorithm is described in detail in [5, 6]. The blurred temporal profile $\tilde{P}(t)$ measured by a TDS and the blurred power spectrum $\tilde{\mathcal{P}}(\omega)$ measured by a spectrometer are the measured data used by the reconstruction algorithm to retrieve the actual pulse profile. The mechanism by which the finite TDS resolution blurs the actual temporal intensity profile $P(t)$ is modeled by a convolution with a Gaussian $G(t)$ of fixed standard deviation R_t

$$(P * G)(t) = \tilde{P}(t). \tag{1}$$

In contrary to [5], in this paper we assume that also the power spectrum $\mathcal{P}(\omega)$ measured by the spectrometer has a limited resolution R_ω. This process is also modeled by a convolution with a Gaussian $G(\omega)$ of width R_ω

$$(\mathcal{P} * G)(\omega) = \tilde{\mathcal{P}}(\omega). \tag{2}$$

The blurred temporal profile $\tilde{P}(t)$ and the blurred power spectrum $\tilde{\mathcal{P}}(\omega)$ are the starting points for the algorithm.

A. Linearly chirped base functions

The electric field of the photon pulse to be approximated is modeled as a sum of in principle arbitrary base functions $B_j(t)$ in time with varying complex coefficients

* florian.christie@desy.de
† Present address: California Institute of Technology, Pasadena, California 91125, USA

$a_{j,m}$, where m is the iteration step,

$$F_m(t) = \sum_{j=1}^{n} a_{j,m} B_j(t) \tag{3}$$

as is the field in the frequency domain

$$\mathcal{F}_m(\omega) = \sum_{j=1}^{n} a_{j,m} \mathcal{B}_j(\omega), \tag{4}$$

where $\mathcal{B}_j(\omega)$ are the base functions in the frequency domain.

The Gaussian base functions described in [5] are not chirped in time as suggested by [7–9]. To accommodate this we introduce an arbitrary linear chirp factor β_j to the base functions

$$B_j(t) = \left(\frac{1}{\sqrt{2\pi}\sigma_j}\right)^{\frac{1}{2}} e^{-\frac{(t-t_j)^2}{4\sigma_j^2}} e^{i\omega_j t} e^{i(t-t_j)^2\beta_j}, \tag{5}$$

where σ_j is the width of the Gaussians centered at times t_j, and the ω_j can be initially calculated based on the energy profile of the electron phase space. For a linearly chirped electron bunch, we can for example set $\omega_j = \omega_0 + 2\frac{\gamma_j - \gamma_0}{\gamma_0}\omega_0$ [10], where ω_0 is the main radiation frequency created by electrons with an energy of γ_0 and γ_j is the mean energy of the electrons around t_j. Otherwise, they are initialized as $\omega_j = \omega_0$.

These base functions are chosen in a way that

$$\begin{aligned}\int_{-\infty}^{\infty} |B_j(t)|^2 \, \mathrm{d}t &= \int_{-\infty}^{\infty} \frac{1}{\sqrt{2\pi}\sigma_j} \cdot e^{-\frac{(t-t_j)^2}{2\sigma_j^2}} \, \mathrm{d}t \\ &= 1.\end{aligned} \tag{6}$$

By setting $C_j = \frac{1}{4\sigma_j^2} - i\beta_j$, Eq. (5) becomes

$$B_j(t) = \left(\frac{1}{\sqrt{2\pi}\sigma_j}\right)^{\frac{1}{2}} e^{-(t-t_j)^2 C_j} e^{i\omega_j t} \tag{7}$$

and we obtain the base functions in frequency domain

$$\mathcal{B}_j(\omega) = \left(\frac{1}{\sqrt{2\pi}\sigma_j}\right)^{\frac{1}{2}} \frac{1}{\sqrt{2C_j}} e^{-\frac{(\omega-\omega_j)(-4iC_j t_j + \omega + \omega_j)}{4C_j}}. \tag{8}$$

Following [8, 9] we set $\beta_j = -\frac{1}{4\sqrt{3}\sigma_j^2}$ for all base functions.

The iteration process and the minimizing is described in detail in [5]. The only change applied to the algorithm is that instead of the actual power spectrum $\mathcal{P}(\omega)$ the blurred power spectrum $\tilde{\mathcal{P}}(\omega)$ is used for the projected spectrum for the real data taken at the Linac Coherent Light Source (LCLS).

B. Testing of the algorithm using a blurred power spectrum

Similar to [5] the algorithm was tested using simulation data of LCLS at 1.5 nm with a blurred power spectrum using a resolution of $R_\omega = 0.2\,\mathrm{eV}$ rms. This value was chosen to match the resolution of the spectrometer used for measurements at LCLS. Therefore, the same tests as in [5] are conducted and showcased in the following using a blurred power spectrum, $(\mathcal{P} * G)(\omega) = \tilde{\mathcal{P}}(\omega)$ with $R_\omega = 0.2\,\mathrm{eV}$.

Simulations of the SASE process in the LCLS undulators at 1.5 nm are conducted using the 1D leap-frog algorithm developed by Z. Huang [8]. Single FEL simulations were run for bunch charges of 20 pC, 40 pC, and 150 pC charge, each resulting in a different X-ray pulse length. Further testing on the code is done using the intensity profiles of 50 different SASE shots right before saturation (using different initial seeds due to the statistical nature of SASE) for a charge of 40 pC.

For each shot 50 reconstructions using different initial base functions are carried out. To obtain the final reconstruction, these 50 reconstructions are then averaged. Figures 1 to 3 show the results for the different bunch charges: the blue solid line is the actual intensity profile from the simulation $P(t)$, the red solid line is the blurred intensity profile $\tilde{P}(t)$ using a resolution of $R_t = 1\,\mathrm{fs}$ in these cases. The black solid line is the mean of the 50 reconstructions surrounded by a light gray shaded area that is one standard deviation. As can be observed, the reconstruction algorithm is still able to retrieve the actual intensity profile very similar to the cases without spectral blurring shown in [5]. The $1 - R^2$ values are all in the same region as in [5] and also the capabilities and limitations of the algorithm remain the same as before.

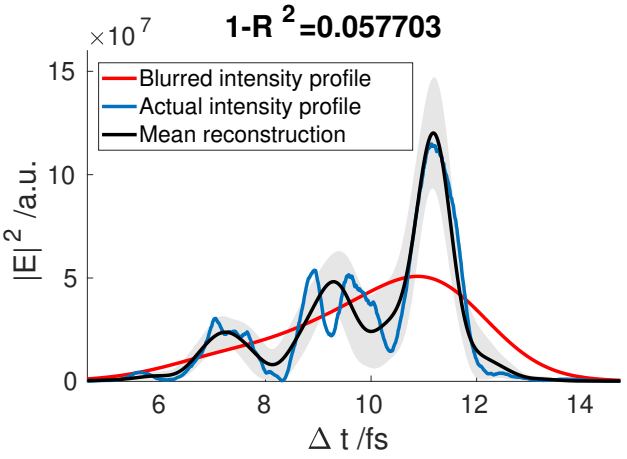


FIG. 1. Reconstruction for 20 pC, $R_t = 1\,\mathrm{fs}$.

Figure 4 shows the $1 - R^2$ values for the 50 different shots with a charge of 40 pC. Comparing to [5] it can be seen, that for every shot the $1 - R^2$ value is in the same order for the perfect and the blurred spectrum, respec-

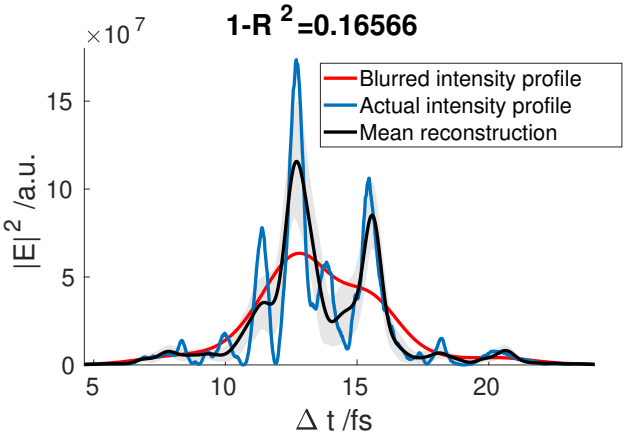


FIG. 2. Reconstruction for 40 pC, $R_t = 1$ fs.

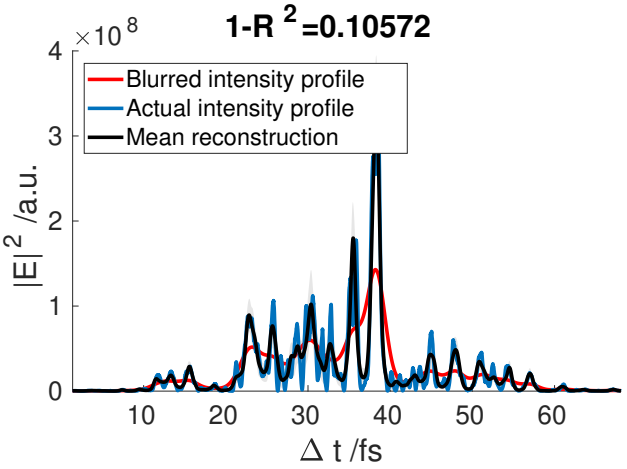


FIG. 3. Reconstruction for 150 pC, $R_t = 1$ fs.

tively. It can therefore be concluded, that the algorithm performs equally well for both spectral measurements.

In summary, the testing results show that the algorithm excels at reconstructing single, isolated spikes and struggles to resolve multiple, dense spikes individually. The existence of adjoining spikes of similar height is retrieved, although the peak power cannot always be correctly determined.

III. ITERATIVE RECONSTRUCTION ALGORITHM APPLIED TO MEASUREMENT DATA TAKEN AT LCLS

A dedicated machine development shift recorded data to be analyzed using the iterative reconstruction.

The measurements were taken at a beam energy of 4 GeV resulting in a wavelength of ~ 1.7 nm or a photon energy of ~ 730 eV. The initial charge at the cathode was 40 pC, which is later collimated to either 20pC or 30pC prior to the undulator. Using energy collimators in the first bunch compressors, electrons with high energy deviations from the reference energy were truncated [11]. An overview of the parameters for the measurements shown in the following can be found in Table I.

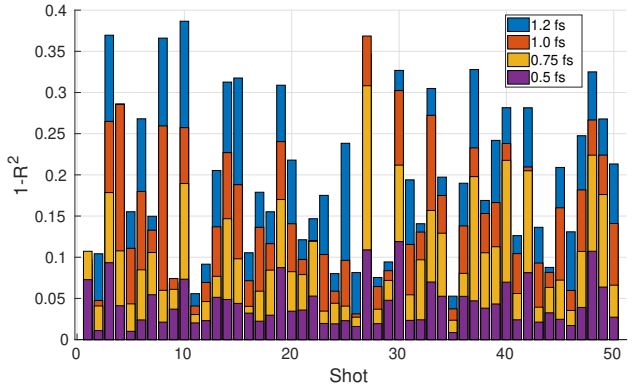


FIG. 4. Results of the reconstruction of 50 different SASE shots for 40 pC bunches for different TDS resolutions shown in the legend. The $1 - R^2$ value is plotted against the shot number. The power spectrum is blurred using a Gaussian blurring of $R_\omega = 0.2$ eV.

TABLE I. Parameter Overview of Measurements for Iterative Reconstruction Algorithm at LCLS

Charge at undulator	30 pC	20 pC
Bunch length σ_t	5 fs	3 fs
Peak current I_e	2.2 kA	2.5 kA
TDS deflecting voltage V	80 MV	80 MV
Temporal resolution R_t	1.2 fs	1.0 fs
Spectral resolution R_ω	0.2 eV	0.2 eV

As the reconstruction has to be performed using bunches that are not yet saturated or close to the saturation point [12], a gain curve was recorded, see Fig. 5. For this reason the beam was kicked behind the 20$^{\text{th}}$ undulator (at $z = 67$ m) to suppress lasing in the downstream undulators. The orbit kick both disrupts overlap between the x-ray waves and electron bunch and degrades electron bunching, interrupting the lasing process [13]. The chosen configuration provided sufficient signal for the spectrometer to work and fulfilled the requirement of being close to the saturation point so that a meaningful reconstruction of the photon pulse power from the energy loss and the energy spread increase of the electron bunch can be performed [12]. The orbit downstream of the undulator section was restored stable by using a closed three-bump [13–15].

To obtain the photon pulse power the longitudinal phase space density of an electron bunch producing light (lasing on) has to be compared to one where the lasing process is suppressed (lasing off). The longitudinal phase space densities are then divided into slices along the time dimension to get the time-dependent beam parameters such as the mean energy $E_{\text{on,off}}(t_i)$, the energy spread $\sigma_{E_{\text{on,off}}}(t_i)$, and the current $I(t_i)$ in each time slice t_i [1, 12]. The subscript denotes, whether the quantity

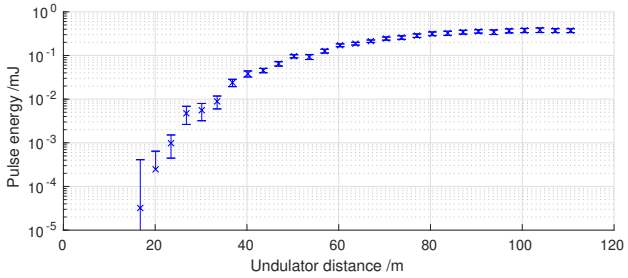


FIG. 5. Gain curve measured at LCLS in the course of recording data for the reconstruction algorithm showing the gas detector signal over the distance traveled in the undulators. The error bars indicate one standard deviation. The beam was kicked behind the 20^{th} undulator (at $z = 67\,\text{m}$) to sustain the unsaturated condition of the bunches, but still provided sufficient signal for the spectrometer.

was taken from a measurement with lasing on or lasing off. The influence of the FEL process on the bunch current is negligible, therefore, this quantity does not have a subscript. For each time slice, the energy loss and the energy spread increase comparing the lasing-on and lasing-off measurement is then calculated

$$\Delta E(t_i) = E_{\text{on}}(t_i) - E_{\text{off}}(t_i), \tag{9}$$

$$\sigma_E(t_i) = \sqrt{\sigma^2_{E_{\text{on}}}(t_i) - \sigma^2_{E_{\text{off}}}(t_i)}. \tag{10}$$

From these quantities the radiation power in each slice can be determined. When using the energy loss method, the radiation power in each slice is [1, 2, 12]

$$P(t_i) = \Delta E(t_i) \cdot \frac{I(t_i)}{e}. \tag{11}$$

When using the energy spread method, the radiation power in each slice is [1, 12, 16]

$$P(t_i) \propto \sigma_E(t_i)^2 \cdot I(t_i)^{\frac{2}{3}}. \tag{12}$$

To determine the total radiation power an additional, independent measurement of the total pulse energy is necessary. This can for example be accomplished using a calibrated gas detector [17–19].

To see if the algorithm reconstructs the photon pulse correctly both, the power profile obtained from the energy loss and the energy spread method, are used as target power profiles for the reconstruction algorithm. By then comparing the reconstructed temporal power profiles one can observe the similarities and differences to check if even though the inputs might be slightly different the algorithm ends up with the same temporal power profile.

In the following, the photon pulses obtained from the reconstruction using only the TDS and the corresponding reconstruction methods are displayed as dashed-dotted lines. The reconstructions using the energy loss method are plotted in black and those using the energy spread method are plotted in blue. 50 different initial guesses serve as starting points for the reconstruction algorithm. These 50 reconstructions are averaged to obtain the final reconstructed photon pulses (solid lines). The mean reconstruction is surrounded by a dark gray and a light gray shaded area which is one standard deviation for the energy loss and the energy spread method, respectively. For the reconstruction the width of the Gaussian base functions σ_j was chosen to be 0.1 fs as well as their spacing $\Delta t = t_{j+1} - t_j$.

A. Reconstruction of photon pulses from bunches with 30 pC charge

We first apply the reconstruction algorithm the experimental data with a charge of 30 pC at the undulator entrance. The parameter overview can be found in the left column of Table I.

Examples of reconstructed photon pulses can be found in Figs. 6 to 8, demonstrating the capabilities and the limitations of the algorithm when applied to measured data. As can be seen in these figures, the photon pulse obtained from the energy loss and the energy spread method differ slightly.

For the power profiles in Fig. 6 the position of most of the larger SASE spikes is the same for both reconstructions. The maximum power of the highest spike is ~ 1.36 times higher if the energy spread method is used as the target profile. This is because the power obtained from the TDS reconstruction at the position of the spike is ~ 1.30 times higher if the energy spread method is used. The smaller SASE spikes agree very well in position and also in height. The reconstruction works well, as the main SASE spikes are separated, which according to Section II B facilitates the reconstruction for the algorithm.

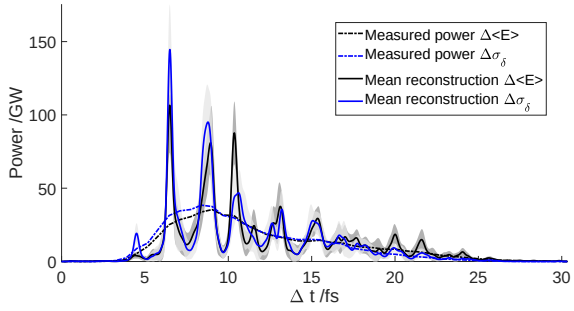


FIG. 6. Reconstruction of a photon pulse measured at LCLS obtained using the iterative reconstruction algorithm, Shot 1. The total bunch charge at the undulator is 30 pC, the TDS resolution is 1.2 fs.

The position and height of most of the main SASE spikes is also very similar for both target profiles shown

in Fig. 7. The maximum power of the main spike differs by less than 7 %. There is a slight difference in the reconstruction on the left side of the main spike. Here, multiple spikes are very close to one another and the reconstruction algorithm reaches its limitations providing slightly different results for the two target profiles. It can be observed that the power profile contains two spikes between 2 fs and 4.5 fs and three between 4.5 fs and 8 fs. The position can be reconstructed, yet the exact maximum power for each single spike remains unknown. The isolated spikes in the region of 10 fs and 20 fs can be retrieved efficiently by the algorithm.

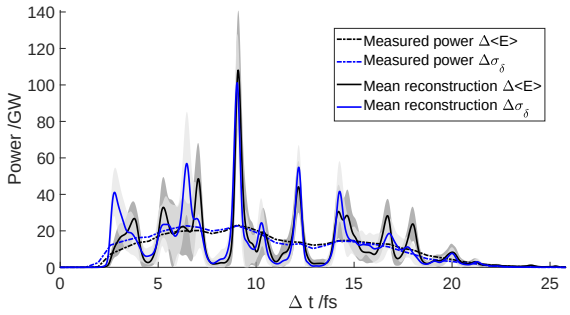


FIG. 7. Reconstruction of a photon pulse measured at LCLS obtained using the iterative reconstruction algorithm, Shot 2. The total bunch charge at the undulator is 30 pC, the TDS resolution is 1.2 fs.

Figure 8 shows a reconstruction where the algorithm reaches the limitations for reconstructing the main features of the photon pulse. These limitations were noted in Section II B. In the central part of the photon pulse (between 6 fs and 10 fs) the SASE spikes are too close to one another to be retrieved by the algorithm. Nonetheless, the smaller, isolated side peaks to the left and right of the central part are retrieved adequately by the algorithm.

B. Reconstruction of photon pulses from bunches with 20 pC charge

Secondly, bunches with a charge of 20 pC at the undulator entrance are used for the reconstruction. The settings are the same as in the previous section, but the bunches are truncated even further using energy collimators in the first bunch compressor. The resulting parameters can be found in the right column of Table I.

Figures 9 to 11 show examples of reconstructed photon pulses for these settings demonstrating the capabilities and the limitations of the algorithm when applied to measured data.

The reconstruction found in Fig. 9 shows a dominant spike at the beginning of the photon pulse. Both methods reconstruct the spike at 2 fs but with a different maximum power. With the energy difference method the power is ∼ 1.35 times higher, in good agreement with

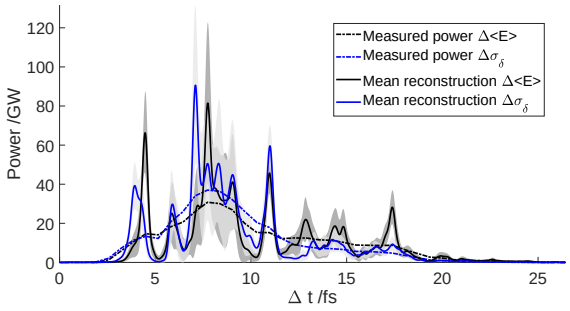


FIG. 8. Reconstruction of a photon pulse measured at LCLS obtained using the iterative reconstruction algorithm, Shot 3. The total bunch charge at the undulator is 30 pC, the TDS resolution is 1.2 fs.

the blurred power, which is ∼ 1.34 times higher. The rest of the photon pulse consists of smaller, dense spikes which can only partly be retrieved by the algorithm. In the region between 8 fs and 10 fs the photon pulse power reconstructed using the energy difference method is close to zero. As a result the algorithm does not reconstruct any power in that region. On the contrary, the energy spread method yields power in this region which results in the reconstruction algorithm showing spikes here. Hence, the difference in the reconstruction is not caused by instability in the algorithm, but rather by the difference in the two TDS analysis methods.

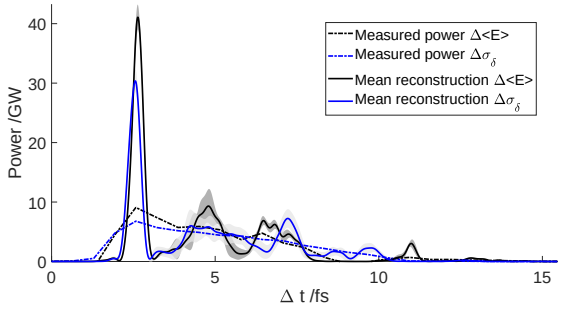


FIG. 9. Reconstruction of a photon pulse measured at LCLS obtained using the iterative reconstruction algorithm, Shot 1. The total bunch charge at the undulator is 20 pC, the TDS resolution is 1.0 fs.

The second example for this setting can be found in Fig. 10. The main spikes between 6 fs and 8 fs and 4 fs and 6 fs of the photon pulse are retrieved using both methods as starting points. The small spike between 2 fs and 3 fs of the photon pulse is higher if the energy spread method is used, as the photon pulse power reconstructed using this method is also higher. Several adjacent spikes in the region of 8 fs to 10 fs cannot be clearly distinguished by the reconstruction algorithm. Additionally, the power obtained by the energy difference method is higher in this region, leading to a higher power retrieved by the algorithm.

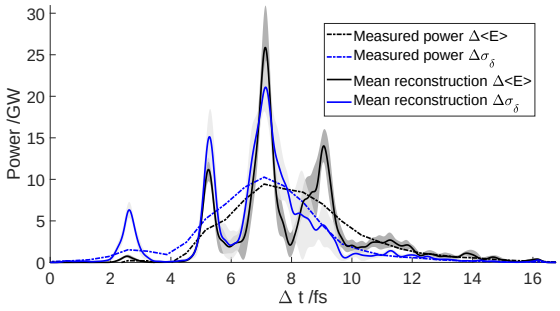


FIG. 10. Reconstruction of a photon pulse measured at LCLS obtained using the iterative reconstruction algorithm, Shot 2. The total bunch charge at the undulator is 20 pC, the TDS resolution is 1.0 fs.

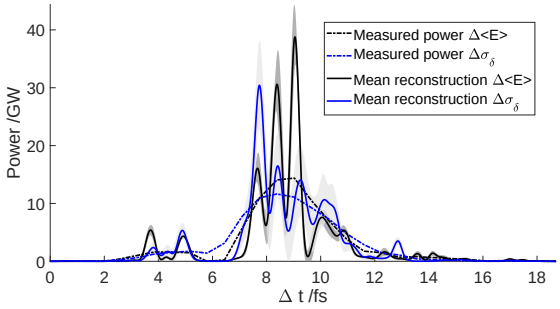


FIG. 11. Reconstruction of a photon pulse measured at LCLS obtained using the iterative reconstruction algorithm, Shot 3. The total bunch charge at the undulator is 20 pC, the TDS resolution is 1.0 fs.

An example where the iterative algorithm did not reconstruct successfully can be found in Fig. 11. Here, the central part of the photon pulse comprises many adjacent SASE spikes that cannot be distinguished by the algorithm. This is expected since the initial reconstruction using the two methods differs in the region of 7 fs to 11 fs both in height and shape and thus, the algorithm ends up with different solutions in this region.

IV. CONCLUSIONS

In this paper, the reconstruction algorithm published in [5] was improved and applied to real measurement data taken at LCLS.

The results show how the reconstruction algorithm using both TDS and spectral information can improve the X-ray pulse profile reconstruction over the established method using only the TDS measurement. The reconstruction accuracy is currently limited by the achievable resolution of the TDS implemented at LCLS. For future upgrades an even better accuracy can be expected. The algorithm excels at reconstructing single, isolated spikes. Multiple, adjacent spikes of similar height are more difficult to be retrieved individually.

ACKNOWLEDGMENTS

This work was supported by the U.S. Department of Energy (DOE) under Contract No. DE-AC02-76SF00515.

This is a pre-print of an article published in Scientific Reports. The final authenticated version is available online at: `https://doi.org/10.1038/s41598-020-66220-5`.

[1] C. Behrens, F.-J. Decker, Y. Ding, V. A. Dolgashev, J. Frisch, Z. Huang, P. Krejcik, H. Loos, A. Lutman, T. J. Maxwell, J. Turner, J. Wang, M.-H. Wang, J. Welch, and J. Wu, Few-femtosecond time-resolved measurements of X-ray free-electron lasers, Nature Communications **5**, 3762 (2014).

[2] Y. Ding, C. Behrens, P. Emma, J. Frisch, Z. Huang, H. Loos, P. Krejcik, and M.-H. Wang, Femtosecond x-ray pulse temporal characterization in free-electron lasers using a transverse deflector, Phys. Rev. ST Accel. Beams **14**, 120701 (2011).

[3] D. Ratner, J. P. Cryan, T. J. Lane, S. Li, and G. Stupakov, Pump-Probe Ghost Imaging with SASE FELs, Phys. Rev. X **9**, 011045 (2019).

[4] D. Zhu, M. Cammarata, J. M. Feldkamp, D. M. Fritz, J. B. Hastings, S. Lee, H. T. Lemke, A. Robert, J. L. Turner, and Y. Feng, A single-shot transmissive spectrometer for hard x-ray free electron lasers, Applied Physics Letters **101**, 034103 (2012).

[5] F. Christie, Y. Ding, Z. Huang, V. A. Jhalani, J. Krzywinski, A. A. Lutman, T. J. Maxwell, D. Ratner, J. Rönsch-Schulenburg, and M. Vogt, Temporal X-ray reconstruction using temporal and spectral measurements, Journal of Physics: Conference Series **1067**, 032011 (2018).

[6] F. Christie, *Generation of Ultra-Short Electron Bunches and FEL Pulses and Characterization of Their Longitudinal Properties at FLASH2*, Ph.D. thesis, Universität Hamburg (2019), DESY-THESIS-2019-022.

[7] R. Bonifacio, L. De Salvo, P. Pierini, N. Piovella, and C. Pellegrini, Spectrum, temporal structure, and fluctuations in a high-gain free-electron laser starting from noise, Phys. Rev. Lett. **73**, 70 (1994).

[8] K.-J. Kim, Z. Huang, and R. Lindberg, *Synchrotron Radiation and Free-Electron Lasers: Principles of Coherent X-Ray Generation* (Cambridge University Press, 2017).

[9] K.-J. Kim, Temporal and transverse coherence of self-amplified spontaneous emission, AIP Conference Proceedings **413**, 3 (1997).

[10] S. Krinsky and Z. Huang, Frequency chirped self-amplified spontaneous-emission free-electron lasers, Phys. Rev. ST Accel. Beams **6**, 050702 (2003).

[11] Y. Ding, K. L. F. Bane, W. Colocho, F.-J. Decker, P. Emma, J. Frisch, M. W. Guetg, Z. Huang, R. Iverson, J. Krzywinski, H. Loos, A. Lutman, T. J. Maxwell, H.-D. Nuhn, D. Ratner, J. Turner, J. Welch, and F. Zhou,

Beam shaping to improve the free-electron laser performance at the Linac Coherent Light Source, Phys. Rev. Accel. Beams **19**, 100703 (2016).

[12] T. J. Maxwell, C. Behrens, Y. Ding, Z. Huang, P. Krejcik, A. Marinelli, L. Piccoli, and D. Ratner, Femtosecond-scale X-ray FEL diagnostics with the LCLS X-band transverse deflector, in *Proc.SPIE*, Vol. 9210 (2014).

[13] D. Ratner, A. Brachmann, F. Decker, Y. Ding, D. Dowell, P. Emma, J. Frisch, S. Gilevich, G. Hays, P. Hering, Z. Huang, R. Iverson, H. Loos, A. Miahnahri, H. Nuhn, J. Turner, J. Welch, W. White, J. Wu, D. Xiang, G. Yocky, and W. M. Fawley, FEL Gain length and Taper Measurements at LCLS, in *Proceedings of FEL2009* (Liverpool, UK, 2009) pp. 221–224.

[14] K. Wille, *The Physics of Particle Accelerators: An Introduction* (Oxford University Press, 2000).

[15] F. Müller, *Compensation of Steerer Crosstalk between FLASH1 and FLASH2*, Master's thesis, Universität Hamburg (2015).

[16] Z. Huang, K. Bane, Y. Cai, A. Chao, R. Hettel, and C. Pellegrini, Steady-state analysis of short-wavelength, high-gain FELs in a large storage ring, Nuclear Instruments and Methods in Physics Research Section A: Accelerators, Spectrometers, Detectors and Associated Equipment **593**, 120 (2008).

[17] K. Tiedtke, A. Azima, N. von Bargen, L. Bittner, S. Bonfigt, S. Düsterer, B. Faatz, U. Frühling, M. Gensch, C. Gerth, N. Guerassimova, U. Hahn, T. Hans, M. Hesse, K. Honkavaar, U. Jastrow, P. Juranic, S. Kapitzki, B. Keitel, T. Kracht, M. Kuhlmann, W. B. Li, M. Martins, T. Núñez, E. Plönjes, H. Redlin, E. L. Saldin, E. A. Schneidmiller, J. R. Schneider, S. Schreiber, N. Stojanovic, F. Tavella, S. Toleikis, R. Treusch, H. Weigelt, M. Wellhöfer, H. Wabnitz, M. V. Yurkov, and J. Feldhaus, The soft x-ray free-electron laser FLASH at DESY: beamlines, diagnostics and end-stations, New Journal of Physics **11**, 023029 (2009).

[18] K. Tiedtke, J. Feldhaus, U. Hahn, U. Jastrow, T. Nunez, T. Tschentscher, S. V. Bobashev, A. A. Sorokin, J. B. Hastings, S. Möller, L. Cibik, A. Gottwald, A. Hoehl, U. Kroth, M. Krumrey, H. Schöppe, G. Ulm, and M. Richter, Gas detectors for X-ray lasers, Journal of Applied Physics **103**, 094511 (2008).

[19] S. Moeller, J. Arthur, A. Brachmann, R. Coffee, F.-J. Decker, Y. Ding, D. Dowell, S. Edstrom, P. Emma, Y. Feng, A. Fisher, J. Frisch, J. Galayda, S. Gilevich, J. Hastings, G. Hays, P. Hering, Z. Huang, R. Iverson, J. Krzywinski, S. Lewis, H. Loos, M. Messerschmidt, A. Miahnahri, H.-D. Nuhn, D. Ratner, J. Rzepiela, D. Schultz, T. Smith, P. Stefan, H. Tompkins, J. Turner, J. Welch, B. White, J. Wu, G. Yocky, R. Bionta, E. Ables, B. Abraham, C. Gardener, K. Fong, S. Friedrich, S. Hau-Riege, K. Kishiyama, T. McCarville, D. McMahon, M. McKernan, L. Ott, M. Pivovaroff, J. Robinson, D. Ryutov, S. Shen, R. Soufli, and G. Pile, Photon beamlines and diagnostics at LCLS, Nuclear Instruments and Methods in Physics Research Section A: Accelerators, Spectrometers, Detectors and Associated Equipment **635**, S6 (2011).